chemosensors

MDPI

Article

A Practical Hydrazine-Carbothioamide-Based Fluorescent Probe for the Detection of Zn^{2+}: Applications to Paper Strip, Zebrafish and Water Samples

Boeon Suh [1], Dongkyun Gil [1], Sojeong Yoon [2], Ki-Tae Kim [2,*] and Cheal Kim [1,*]

[1] Department of Fine Chem, Seoul National University of Science and Technology, Seoul 01811, Korea; ssbbee95@naver.com (B.S.); prmodel0131@seoultech.ac.kr (D.G.)
[2] Department of Environment Engineering, Seoul National University of Science and Technology, Seoul 01166, Korea; sojung5571@gmail.com
* Correspondence: ktkim@snut.ac.kr (K.-T.K.); chealkim@snut.ac.kr (C.K.); Tel.: +82-2-962-6642 (K.-T.K.); +82-2-971-6680 (C.K.); Fax: +82-2-972-9149 (K.-T.K.)

Abstract: A practical hydrazine-carbothioamide-based fluorescent chemosensor **TCC** (N-(4-chlorophenyl)-2-(thiophene-2-carbonyl)hydrazine-1-carbothioamide) was applied for Zn^{2+} detection. **TCC** exhibited selective fluorescence emission for Zn^{2+} and did not show any interference with other metal ions. In particular, **TCC** was utilized for the detection of Zn^{2+} in paper strips, zebrafish and real water samples. **TCC** could detect Zn^{2+} down to 0.39 μM in the solution phase and 51.13 μM in zebrafish. The association ratio between **TCC** and Zn^{2+} was determined to be 2:1 by ESI-mass and Job plot. The sensing mechanism of **TCC** for Zn^{2+} was illustrated to be a chelation-enhanced fluorescence process through spectroscopic experiments and theoretical calculations.

Keywords: zinc ion; hydrazine; chemosensor; carbothioamide; zebrafish; test-strip

check for updates

Citation: Suh, B.; Gil, D.; Yoon, S.; Kim, K.-T.; Kim, C. A Practical Hydrazine-Carbothioamide-Based Fluorescent Probe for the Detection of Zn^{2+}: Applications to Paper Strip, Zebrafish and Water Samples. *Chemosensors* **2022**, *10*, 32. https://doi.org/10.3390/chemosensors10010032

Academic Editor: Guo-Hui Pan

Received: 30 November 2021
Accepted: 10 January 2022
Published: 12 January 2022

1. Introduction

Zinc is a crucial trace nutrient for organisms and the second-most plentiful transition metal in the body [1–4]. For decades, zinc has been noted for its pivotal roles involved in biological processes, such as the growth of living organisms, neural signal transmission and gene transcription [5–8]. Due to the various functions of zinc in biological processes, however, an unbalance of zinc has been associated with various pathological troubles [9–11].

Particularly, zinc deficiency in the human body results in a severe effect on impaired taste, depressed immunity, delayed sexual maturation and growth defects [12]. In contrast, too much zinc can lead to neurodegenerative damage, including infantile diarrhea, Alzheimer's disease, diabetes and Parkinson's disease [13,14]. Thus, there is an imperative need to develop tools that can prevent undue exposure to zinc in living organisms.

The zinc detection methods reported thus far include atomic absorption spectrometry, electrochemistry, potentiometry and fluorescence spectroscopy [15–22]. Among them, chemosensors based on fluorescence spectroscopy have been a useful method for sensing of Zn^{2+} due to the fast response, high selectivity and sensitivity, ease of manipulation and bioimaging ability [23–26].

Hitherto, several studies have reported that fluorescent probes based on naphthalene, coumarin, phenanthrene, anthracene, rhodamine, antipyrine and triazole have been applied to the sensing of Zn^{2+} [27–33]. However, there are still many disadvantages, such as complex synthesis processes and difficulty in bioimaging. Thus, it is necessary to develop an easily accessible fluorescent chemosensor for detecting zinc in biological systems.

Thiourea has attracted attention for its capability to bind to metals [34,35]. In particular, the sulfur atom in thiourea prefers to chelate with soft metal ions, such as Zn^{2+} and Hg^{2+}, through the hard-soft acid base theory [36–38]. In order to selectively detect only Zn^{2+} with

the thiourea moiety, we intended to endow a hard character to the thiourea by combination with hydrazine with hard base nitrogen atoms [39,40].

Moreover, hydrazine has a water-soluble character [41]. To keep these properties in mind, we designed and found the compound **TCC,** including the thiourea and hydrazine moieties, as reported in the literature [42,43]. We applied **TCC** as a sensor with the expectation that it could coordinate well to zinc ion and might be soluble in water for biological applications.

Herein, we address a practical hydrazine-carbothioamide-based fluorescent sensor **TCC** for detecting Zn^{2+}. **TCC** exhibited selective fluorescence emission for only Zn^{2+} and all the other cations did not interfere with the fluorescence emission of **TCC** to Zn^{2+}. Significantly, **TCC** was a suitable chemosensor capable of detecting Zn^{2+} with practical applications, such as real water samples, paper-strips and zebrafish. **TCC** could detect down to 0.39 μM of Zn^{2+} in the solution phase and 51.13 μM of Zn^{2+} in zebrafish. The sensing interaction of **TCC** for Zn^{2+} was demonstrated by ESI-mass, ^{1}H NMR titration, calculations, fluorescent experiments and UV-vis titration.

2. Experiments

2.1. Materials and Equipment

All the chemicals were supplied by Sigma–Aldrich (Burlington, MA, USA). A Varian spectrometer was employed to obtain ^{1}H NMR and ^{13}C NMR. Perkin Elmer model spectrometers were employed to obtain the absorption and fluorescent spectra. ESI-mass measurements were conducted using a Thermo MAX instrument (Molecular Devices, San Jose, CA, USA).

2.2. Synthesis of TCC (N-(4-Chlorophenyl)-2-(thiophene-2-carbonyl)hydrazine-1-carbothioamide)

The compound **TCC** reported in the literature [42,43] was synthesized in reaction solvent acetonitrile as follows (Scheme 1). Thiophene-2-carbohydrazide (128 mg, 9.0×10^{-4} mol) and 1-chloro-4-isothiocyanatobenzene (170 mg, 1.0×10^{-3} mol) were dissolved in 5.0 mL acetonitrile. The resulting solution was shaken for 2 h at room temperature. The white powder produced was collected by filtration, washed with diethyl ether and dried at 60 °C for 4 h (yield: 75%).

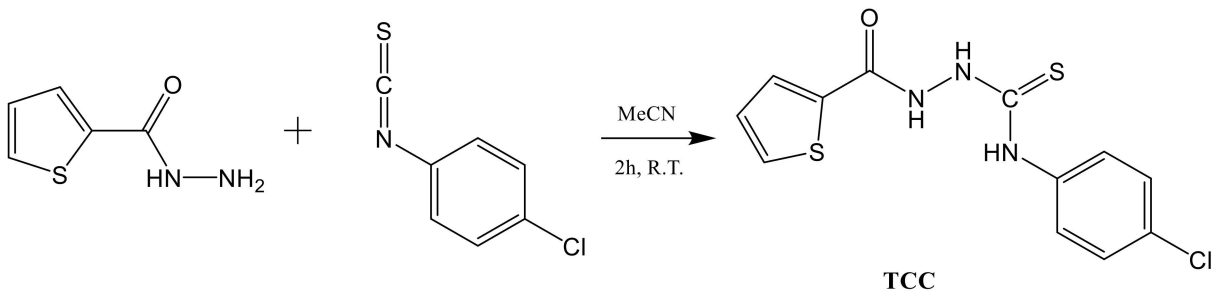

Scheme 1. The synthesis of **TCC**.

TCC was affirmed by ^{1}H, ^{13}C NMR and ESI-MS (Figures S1–S3). ^{1}H NMR (DMSO-d_6): 10.60 (s, 1H), 9.95 (s, 1H), 9.92 (s, 1H), 7.87 (d, 2H), 7.60 (s, 1H), 7.47 (d, 1H), 7.35 (t, 1H), 7.21 (d, 2H). ^{13}C NMR (DMSO-d_6): 140.73 (1C), 137.33 (1C), 131.73 (2C), 129.55 (3C), 127.99 (2C) and 124.73 (3C). ESI-MS for [**TCC** + H^+ + H_2O]$^+$, calcd, 330.01 (*m/z*); found, 330.08. Water solubility of **TCC**: 0.11 g/L (Figure S4).

2.3. Fluorescent and UV-Vis Titrations

TCC (3.1 mg, 2.0×10^{-5} mol) was dissolved in 1.0 mL DMF to make a stock (2.0×10^{-2} M). We added 6 μL of the **TCC** stock to 2.990 mL bis-tris buffer (1×10^{-2} M, pH 7.0) to make 40 μM. $Zn(NO_3)_2$ (15.2 mg, 5×10^{-5} mol) was dissolved in 5 mL buffer to make a Zn^{2+} stock

(1.0×10^{-2} M). We added 1.2–20.4 μL of the Zn^{2+} stock to **TCC** (40 μM). After blending them for 5 s, their fluorescent and UV-vis data were obtained.

2.4. Job Plot

Two stock solutions, **TCC** (2.0×10^{-2} M) and Zn^{2+} (1.0×10^{-2} M), were prepared as described in titration section. We diluted 100 μL of the **TCC** stock in 49.9 mL buffer to give 4×10^{-5} M, and 200 μL of the Zn^{2+} stock was diluted to 49.9 mL buffer to afford 4×10^{-5} M. We delivered 0.3–2.7 mL of the diluted **TCC** to the UV-vis cell. The diluted Zn^{2+} was delivered to the cells to provide 3 mL. After blending them for 5 s, fluorescent data were obtained.

2.5. Competitive Tests

The **TCC** (40 μM) solution was prepared as mentioned in the titration section. To provide metal stocks (1.0×10^{-2} M), $5x10^{-5}$ mol of various cations (Zn^{2+}, K^{+}, Pb^{2+}, Na^{+}, Cu^{2+}, Hg^{2+}, Fe^{2+}, Cd^{2+}, Mn^{2+}, Mg^{2+}, Ca^{2+}, Ni^{2+}, Ga^{3+}, Cr^{3+}, Fe^{3+}, Co^{3+}, In^{3+} and Al^{3+}) was dissolved separately in 5 mL of buffer. We added 19.2 μL of each metal stock (1.0×10^{-2} M) into **TCC** (40 μM). Then, 19.2 μL of $Zn(NO_3)_2$ stock (1.0×10^{-2} M) was delivered to the mixed solution of **TCC** and each metal. Fluorescent data were obtained after blending them for 5 s.

2.6. ^{1}H NMR Titration

Four NMR glass tubes of **TCC** (3.1 mg, 1.0×10^{-5} mol) dissolved in deuterated DMF (1.0 mL) were prepared. We added 0–20 μL (0–2.0 equiv) of Zn^{2+} dissolved in deuterated DMF to the **TCC**. After blending these for 5 s, their ^{1}H NMR spectra were obtained.

2.7. pH Test

A diverse pH range (6–9) of buffer solutions was prepared by mixing KOH and HCl in Tris-HCl buffer and bis-tris buffer. We placed 6 μL of **TCC** (2.0×10^{-2} M) stock into 2.99 mL buffer solutions to produce 4.0×10^{-5} M. We added 19.2 μL of a Zn^{2+} solution (1.0×10^{-2} M) to each **TCC** solution (4.0×10^{-5} M). After blending them for 5 s, fluorescent data were obtained.

2.8. Water Sample

To analyze the utilization of **TCC** for Zn^{2+} in real water samples, tap and drinking water were prepared in our laboratory. A **TCC** stock (2.0×10^{-2} M) was prepared as described in titration section. We added 6 μL of the **TCC** stock to a 2.99 mL water sample containing Zn^{2+} (8.00 μM). After blending for 5 s, fluorescent data were obtained.

2.9. Fluorescent Paper-Strips

The **TCC**-paper strips were provided by soaking the filter papers in **TCC** (2×10^{-2} M, DMF) and drying them. **TCC**-paper strips were added to 1 mM of metal ions in buffer. After drying, their photographs were taken.

2.10. Zebrafish Imaging

The 6-day-old zebrafish were reared under our former conditions [44]. Before proceeding with the imaging experiment, we prepared a **TCC** stock (2.0×10^{-2} M) and a Zn^{2+} stock (1.0×10^{-2} M). We added 50 μL of the **TCC** stock to 19.95 mL E2 media. The zebrafish were incubated with **TCC** (50 μM) in E2 media with 0.3% DMSO for 15 min and then washed with E2 media.

The zebrafish were separated into four groups. One was a control group, and the other groups were further treated with 150, 250 or 500 μM of Zn^{2+} for 15 min. The zebrafish were anesthetized by ethyl-3-aminobenzoate methanesulfonate. A few seconds later, we conducted all the imaging experiments using a fluorescence microscope. With Icy software, the mean fluorescence intensity of the images was analyzed.

2.11. Theoretical Studies

Theoretical calculations for **TCC** and **TCC**-Zn^{2+} were studied using the Gaussian 16 program [45]. The DFT method was employed for geometry optimizations [46,47]. The B3LYP and 6–31G(d,p) basis set was employed for all atoms except Zn^{2+} [48,49]. In the case of **TCC**-Zn^{2+}, the LANL2DZ basis set was applied to Zn^{2+} [50–52]. None of the imaginary frequency appeared in the optimized-patterns and local minima of **TCC** and **TCC**-Zn^{2+} were verified. The solvent effect of water was dealt with IEFPCM [53]. The thirty probable UV-vis transition states were calculated with the TD-DFT method based on the energy-optimized patterns of **TCC** and **TCC**-Zn^{2+}.

3. Results and Discussion

3.1. Fluorescence Investigation of TCC to Zn^{2+}

To identify the selectivity of **TCC** toward various cations (Zn^{2+}, K^{+}, Pb^{2+}, Na^{+}, Cu^{2+}, Hg^{2+}, Fe^{2+}, Cd^{2+}, Mn^{2+}, Mg^{2+}, Ca^{2+}, Ni^{2+}, Ga^{3+}, C^{3+}, Fe^{3+}, Co^{3+}, In^{3+} and Al^{3+}) the fluorescent response was tested in bis-tris buffer (Figure 1). With excitation at 320 nm, **TCC** displayed no fluorescence around 450 nm (λ_{ex} = 320 nm, Φ = 0.0258).

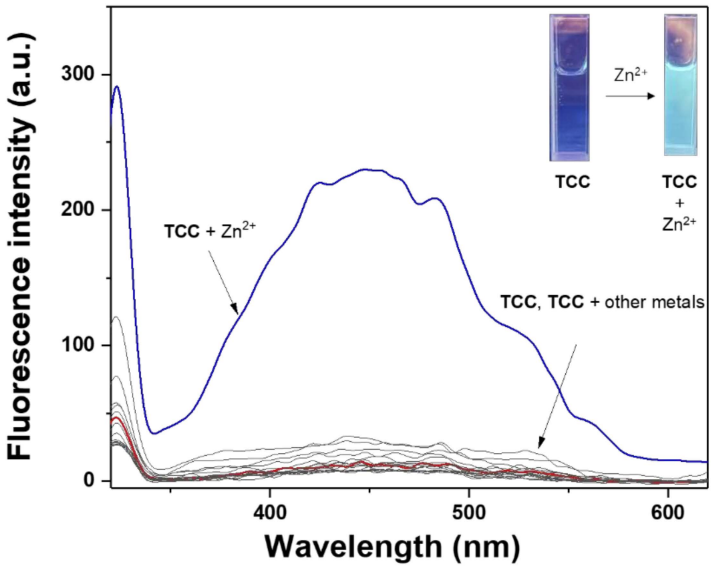

Figure 1. Fluorescence spectral response of **TCC** (4.0×10^{-5} M) toward diverse metal ions (Zn^{2+}, K^{+}, Pb^{2+}, Na^{+}, Cu^{2+}, Hg^{2+}, Fe^{2+}, Cd^{2+}, Mn^{2+}, Mg^{2+}, Ca^{2+}, Ni^{2+}, Ga^{3+}, Cr^{3+}, Fe^{3+}, Co^{3+}, In^{3+} and Al^{3+}; λ_{ex} = 320 nm). Inset: Fluorescent pictures of **TCC** (4.0×10^{-5} M) and **TCC** (4.0×10^{-5} M) with Zn^{2+} (1.6 equiv).

When each cation (1.6 equiv) was added to **TCC**, only Zn^{2+} rapidly induced remarkable fluorescence emission at 450 nm (Φ = 0.1255). There was no fluorescence emission with the other analytes, indicating that **TCC** may work as a selective fluorescent probe for detecting Zn^{2+}. On the other hand, the quenching effect of S^{2-} and pyrophosphate (PPi) to **TCC**-Zn^{2+} was examined, but no fluorescence change occurred.

Fluorescence and UV-vis titrations were conducted to examine the sensing property of **TCC** for Zn^{2+} (Figures 2 and 3). As different concentrations of Zn^{2+} (0–1.7 equiv) were added to **TCC**, the fluorescence emission at 450 nm constantly increased until 1.6 equiv of Zn^{2+} was added. UV-vis titration was also performed under the same condition. Upon addition of Zn^{2+} into **TCC**, the absorbance of 340 nm consistently increased and that of 270 nm decreased until Zn^{2+} reached at 1.6 equiv. There was an evident isosbestic point at 288 nm, which signifies that the interaction of **TCC** and Zn^{2+} provided a product.

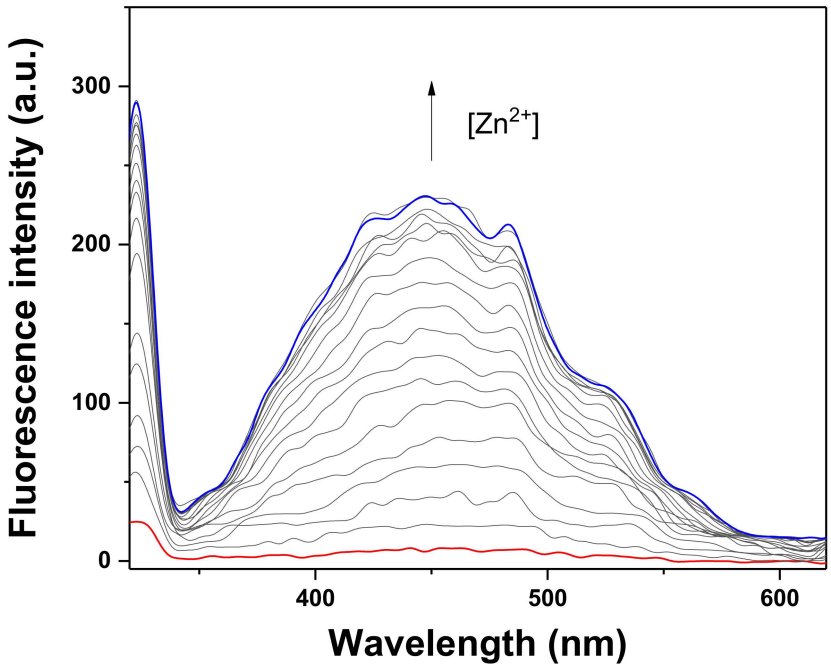

Figure 2. Fluorescence spectral response of **TCC** (4.0×10^{-5} M) with varied concentrations of Zn^{2+} (λ_{ex} = 320 nm). The arrow from bottom to top represents that fluorescence emission increased with the increasing Zn^{2+} (0, 4, 8, 12,16, 20, 24, 28, 32, 36, 40, 44, 48, 52, 56, 60, 64 and 68 μM).

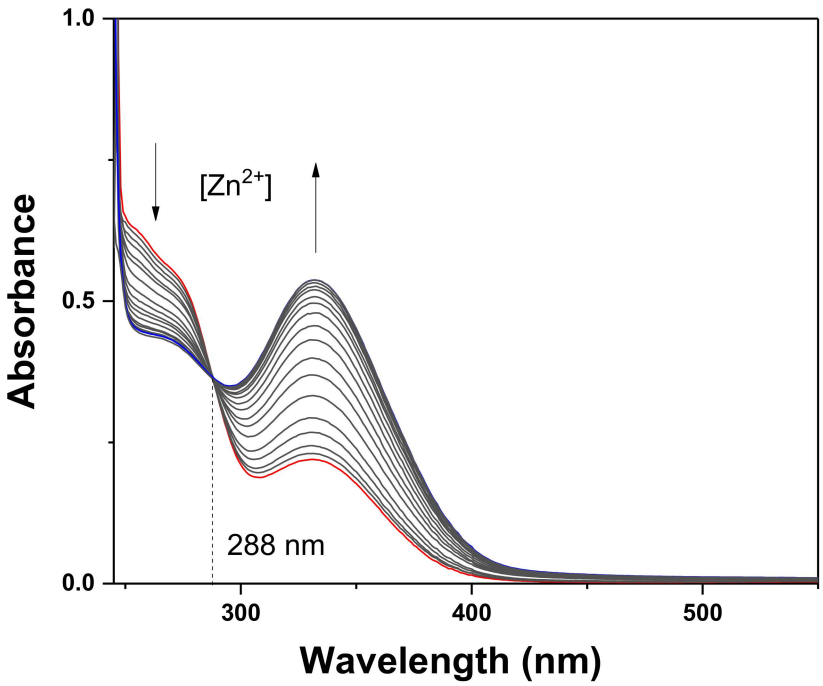

Figure 3. Absorption variations of **TCC** (4.0×10^{-5} M) with varied concentrations of Zn^{2+}. As indicated by the arrow, the absorption of 270 nm gradually decreased with the increasing Zn^{2+} (0, 4, 8, 12, 16, 20, 24, 28, 32, 36, 40, 44, 48, 52, 56, 60, 64 and 68 μM), while the absorption of 340 nm increased.

A Job plot was employed to apprehend the association ratio of **TCC** for Zn^{2+} (Figure 4). The greatest fluorescence emission at 450 nm appeared at a molar fraction of 0.7, which means that **TCC** and Zn^{2+} formed a complex with a 2:1 association ratio. The ratio was also proven by ESI-MS (Figure S5). The peak of 725.82 (*m/z*) corresponded to [2·**TCC** − H^+ + Zn^{2+} + MeCN]$^+$ (calculated *m/z* = 725.94) in the positive-ion spectrum.

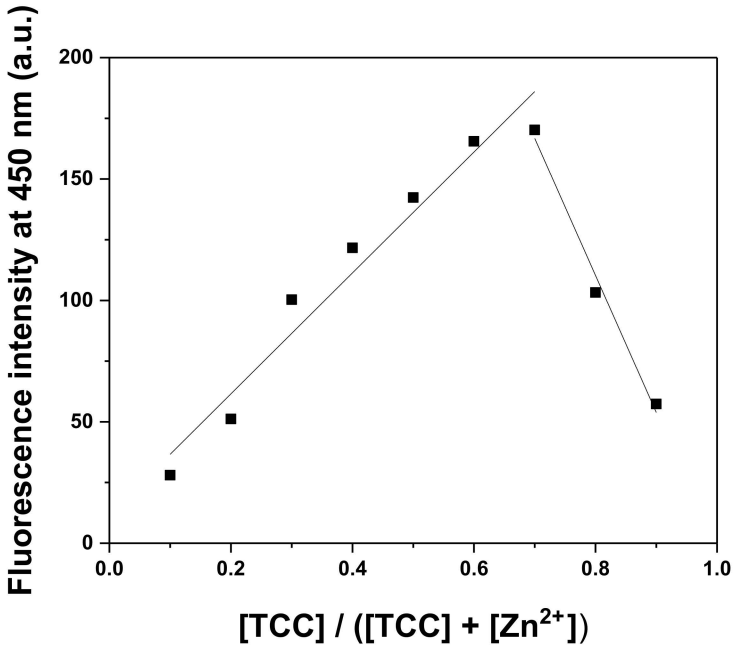

Figure 4. A Job plot for **TCC** with Zn^{2+} (λ_{ex} = 320 nm).

From the definition of IUPAC ($C_{DL} = 3\sigma/k$) [54], the detection limit for Zn^{2+} was calculated to be 0.39 μM (Figure 5). This was much lower than the drinking water standard (76 μM) stipulated by the World Health Organization (WHO) [55]. More importantly, the value is the lowest among those formerly addressed for hydrazine-carbothioamide-based fluorescent Zn^{2+} chemosensors (Table S1) [34,39,56–58]. The association constant (K) of **TCC**-Zn^{2+} was given as 2×10^8 M^{-2} from Li's equation (Figure S6).

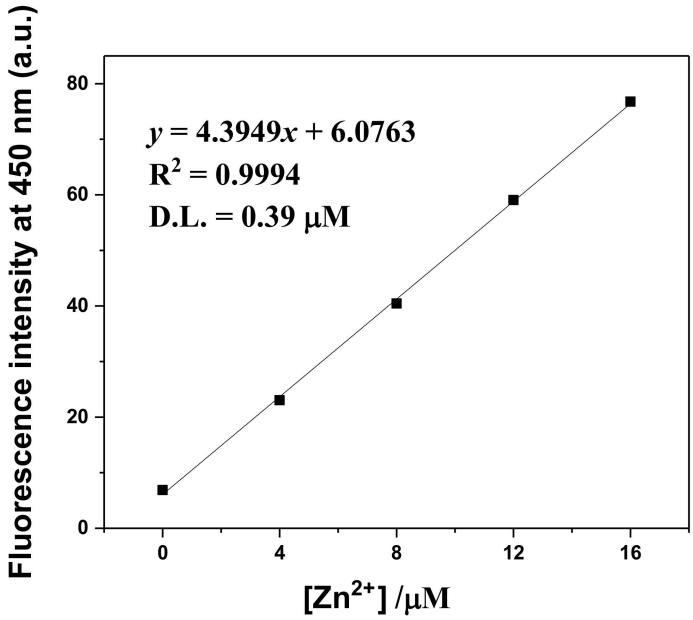

Figure 5. The detection limit for Zn^{2+} by **TCC** (4.0×10^{-5} M) based on the fluorescence emission at 450 nm (λ_{ex} = 320 nm).

To determine an appropriate sensing mechanism between **TCC** and Zn^{2+}, ^{1}H NMR titrations were conducted (Figure S7). When 0.5 equiv of Zn^{2+} was added to **TCC**, the peak of thiourea protons (H_4, H_5 and H_6) shifted downfield. Upon the addition of Zn^{2+} up to 2.0 equiv, the integral value of H_4 decreased to half, indicating that the proton H_4 of one

of two **TCC** molecules was deprotonated by binding with Zn^{2+}. Thus, we predicted that both the nitrogen of amide and the sulfur of thiourea would bind to Zn^{2+}. Based on the results of the ESI-mass, Job plot and ^{1}H NMR titration, a proper structure of Zn^{2+}-2·**TCC** was suggested (Scheme 2).

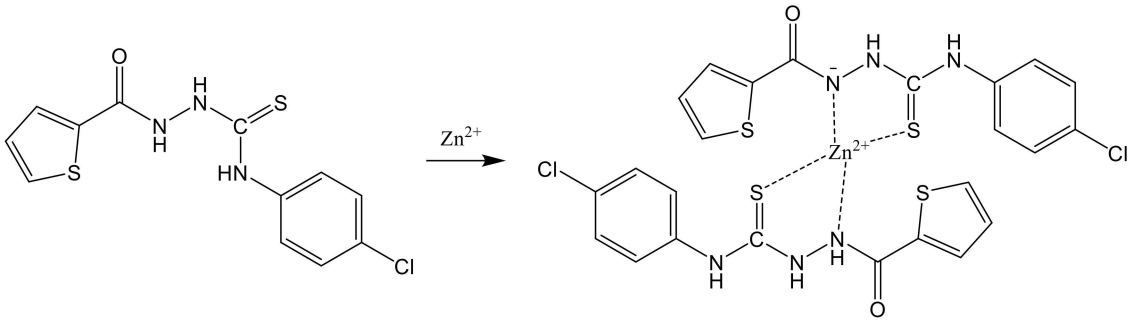

Scheme 2. The proposed response mechanism of **TCC** for Zn^{2+}.

A competition test was performed to understand a probing ability of **TCC** toward Zn^{2+}. The fluorescent spectra of **TCC** were recorded in the presence of Zn^{2+} along with other cations (Figure 6). There was no interference in the fluorescent spectra of **TCC** for detecting Zn^{2+}, indicating that **TCC** was an excellent sensor to detect Zn^{2+} without interference from other cations. The pH test of **TCC** and Zn^{2+}-2·**TCC** was conducted in different pH conditions (pH 6–9) (Figure S8). For **TCC**, there was no fluorescence emission from pH 6 to 9. Meanwhile, the fluorescence intensity of Zn^{2+}-2·**TCC** was prominently increased between pH 7 and 9. This outcome signified that **TCC** may be utilized for sensing Zn^{2+} at pH 7–9.

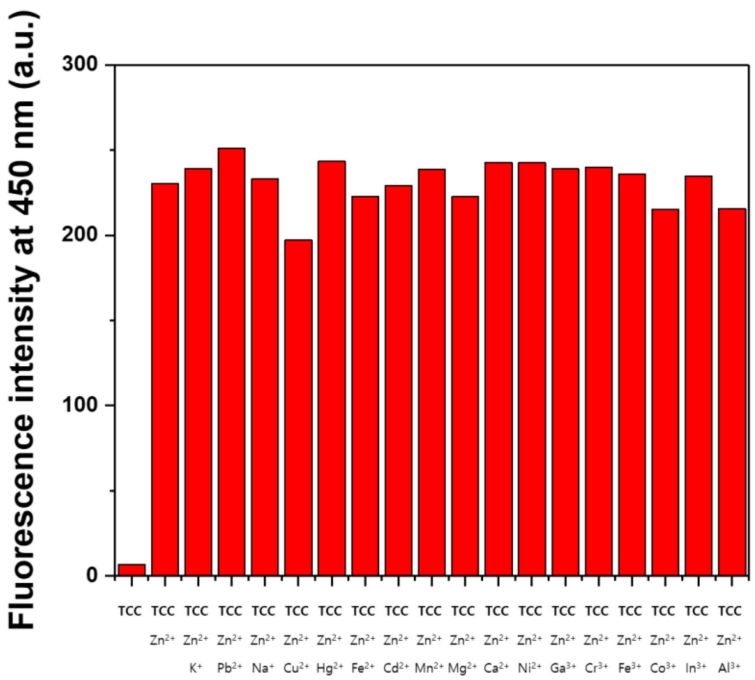

Figure 6. The fluorescence intensity for the reaction of **TCC** (4.0×10^{-5} M) at 450 nm with the addition of Zn^{2+} (1.6 equiv) with/without other metal ions (1.6 equiv; λ_{ex} = 320 nm).

To ensure the practical availability of **TCC**, a fluorescent paper-strip application was performed under fluorescence lamp (λ_{ex} = 365 nm) (Figure 7). Among the various metals, **TCC** could detect only Zn^{2+} with definite fluorescent emission. The results suggested that **TCC** was able to detect Zn^{2+} in the paper-applied phase. The application of **TCC**

in real samples was conducted to inspect the practical utility of **TCC** (Table 1). Reliable recoveries and R.S.D. values were observed in both drinking and tap water samples, meaning that **TCC** has a great potential to be employed as a reliable tool for monitoring Zn^{2+} in real samples.

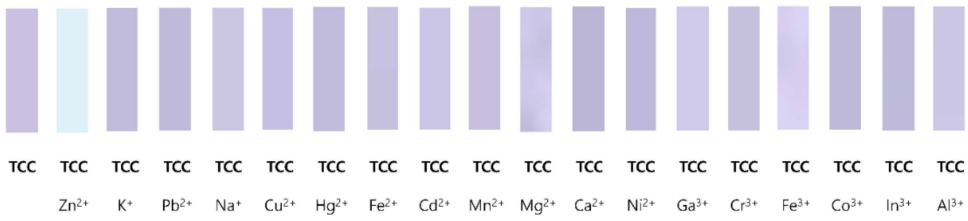

Figure 7. Photographs of **TCC**-paper strips dipped in varied metal ions.

Table 1. The determination of Zn^{2+} [a].

Sample	Zn^{2+} Added (μM)	Zn^{2+} Found (μM)	Recovery (%)	R.S.D. (*n* = 3) (%)
Drinking water	0.0	*n.d.		
	8.00 [b]	8.25	103.12	0.94
Tap water	0.0	*n.d.		
	8.00 [b]	7.90	98.75	0.19

[a] Conditions: [**TCC**] = 40 μM in buffer. [b] 8 μM of Zn^{2+} was artificially added. *n.d.: Not detected.

3.2. Imaging in Zebrafish

To identify the biological applications of **TCC** for Zn^{2+}, imaging experiments were achieved with zebrafish (Figure 8). When the zebrafish were treated with **TCC** (50 μM) for 15 min, there was no fluorescence in the swim bladder (Figure 8(a_2)). However, as the amounts of Zn^{2+} increased to 150, 250 and 500 μM (Figure 8(b_2–d_2)), the fluorescence in the swim bladder gradually increased. In the swim bladder, the detection limit for Zn^{2+} was analyzed to be 51.13 μM with the Icy software (Figure S9). These results illustrate that **TCC** may be applied to trace Zn^{2+} in live organisms.

3.3. Calculations

Optimized patterns of **TCC** and Zn^{2+}-2·**TCC** were investigated according to the analyses of the ESI-mass and Job plot. As shown in Figure 9, **TCC** had a twist structure with a dihedral angle of −101.27° for 1C, 2N, 3N and 4C, whereas the coordination of Zn^{2+} to two **TCC** molecules displayed a more rigid tetrahedral structure (dihedral angle = 175.18°). The bond distances related to coordination of Zn^{2+} to **TCC** were calculated to be 1.992 Å for 2N-Zn^{2+} and 2.341 Å for 5S-Zn^{2+}, which are in the range of the general bond distances for binding with Zn^{2+} [59,60].

TD-DFT calculations were achieved based on energy-optimized patterns of **TCC** and Zn^{2+}-2·**TCC** complex. The leading absorption of **TCC** at 259.1 nm was caused from the HOMO-3 → LUMO (61%), HOMO-4 → LUMO (17%) and HOMO-6 → LUMO (13%) transitions, which are related to the $\pi \rightarrow \pi^*$ transition (Figures S10 and S11). For the Zn^{2+}-2·**TCC** complex, an absorption band related to the red-shift originated from the HOMO → LUMO+2 (96%) transition (319.9 nm, Figures S11 and S12) and exhibited a $\pi \rightarrow \pi^*$ transition. The red-shift recorded in the UV-vis spectra corresponded well with the calculated transition states.

Both **TCC** and its complex state showed similar transition characters, and the rigidity in the complex state of **TCC** increased. Thus, fluorescent 'turn-on' sensing would be caused by chelation-enhanced fluorescence process [61]. When **TCC** was converted into the complex state with Zn^{2+}, the reduction of nonradiative transitions, such as rotations and vibrations, would lead to the enhancement of radiative transitions, like fluorescence.

Referring to various spectroscopic experiments and theoretical calculations, we present a plausible sensing model of Zn^{2+} by **TCC** (Scheme 2).

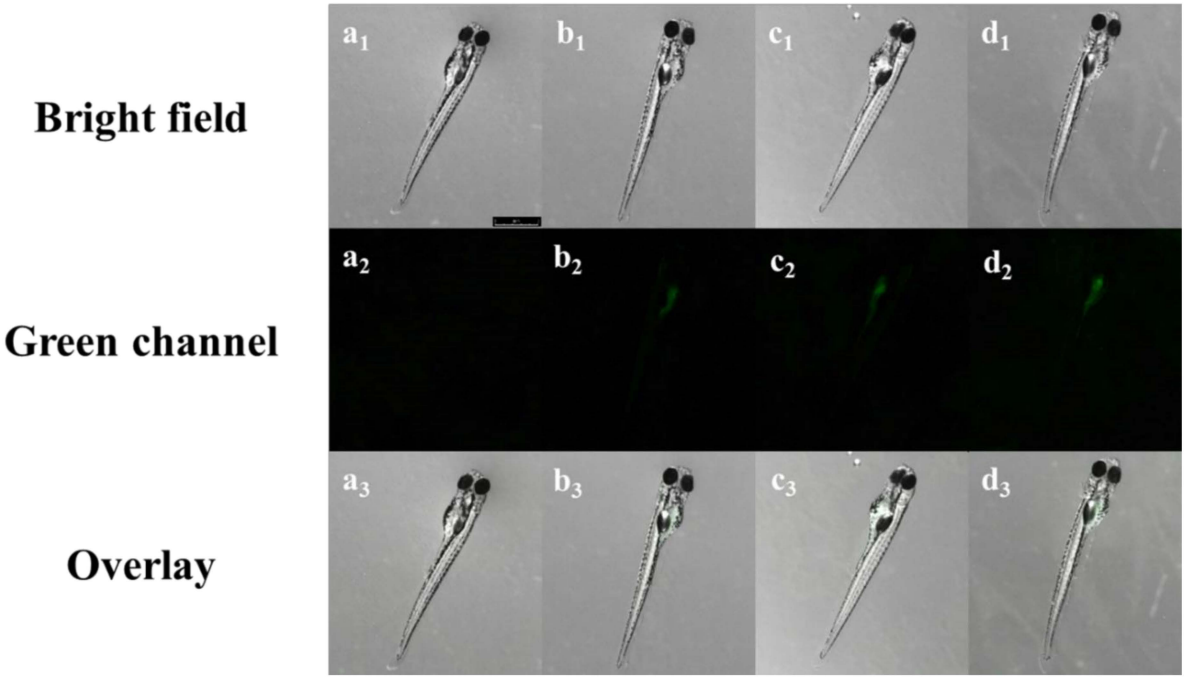

Figure 8. Fluorescence images of 6-day-old zebrafish exposed to **TCC** followed by the addition of Zn^{2+}. (**a**$_1$–**a**$_3$): **TCC** only; (**b**$_1$–**b**$_3$): **TCC** with 150 μM Zn^{2+}; (**c**$_1$–**c**$_3$): **TCC** with 250 μM Zn^{2+}; and (**d**$_1$–**d**$_3$): **TCC** with 500 μM Zn^{2+}. [**TCC**] = 50 μM. Scale bar: 2.00 mm.

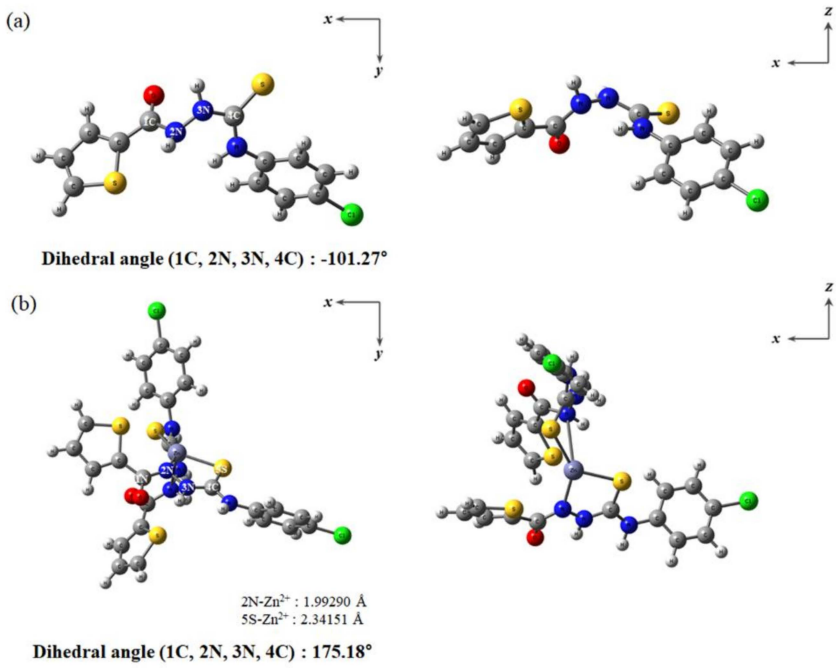

Figure 9. Energy-optimized patterns of (**a**) **TCC** and (**b**) Zn^{2+}-2·**TCC**.

4. Conclusions

We presented a practical hydrazine-carbothioamide-based fluorescent chemosensor **TCC** that could effectively detect Zn^{2+} in aqueous media. Probe **TCC** could detect Zn^{2+} among the other metal ions through selective fluorescence emission. In addition, **TCC**

could clearly recognize Zn^{2+} with competition from metal ions. Particularly, **TCC** could be used as a practical probe capable of detecting Zn^{2+} in paper-strip, zebrafish and real water samples.

The detection limit of **TCC** for Zn^{2+} was calculated to be 0.39 μM in the solution phase and 51.13 μM in zebrafish. Importantly, the value in the solution phase is the lowest among those formerly addressed for hydrazine-carbothioamide-based fluorescent Zn^{2+} chemosensors. The binding mode of **TCC** for Zn^{2+} was revealed to be a 2:1 by the Job plot and ESI-mass. The detecting mechanism of **TCC** toward Zn^{2+} was described as the chelation-enhanced fluorescence process based on the results of spectroscopic studies and theoretical calculations.

Future study will focus on the development of hydrazine-carbothioamide-based chemosensors, which may operate at long excitation wavelengths for fluorescence bio-imaging. In addition, we will consider the development of an integrated system with portable fluorescent recognition or smartphone-based sensors [62,63].

Supplementary Materials: The following supporting information can be downloaded at: https://www.mdpi.com/article/10.3390/chemosensors10010032/s1, Table S1: Examples of hydrazine-carbothioamide-based fluorescence chemosensors for detecting Zn^{2+}. Figure S1: ^{1}H NMR spectrum of **TCC**. Figure S2: ^{13}C NMR spectrum of **TCC**. Figure S3: Positive-ion ESI-mass spectrum of **TCC** (100 μM). Figure S4: Solubility of **TCC** in distilled water based on the absorbance at 320 nm. Solubility was calculated to the **TCC**-saturated solution with linear fitting curve of **TCC** (0, 40, 80, 120, 160 and 200 μM). Figure S5: Positive-ion ESI-mass spectrum of **TCC** (100 μM) upon the addition of Zn^{2+} (1 equiv). Figure S6: Li's equation plot (at 450 nm) of **TCC** (40 μM) based on fluorescence titration, assuming 2:1 stoichiometry for association between **TCC** and Zn^{2+}. Figure S7: ^{1}H NMR titration of **TCC** (10 mM) upon the addition of different amounts of Zn^{2+} (0–2.0 equiv). Figure S8: Fluorescence intensity of **TCC** and **TCC**-Zn^{2+} at a pH range of 6 to 9. Figure S9: Quantification of the mean fluorescence intensity in Figure 8a_2–d_2. Figure S10: (a) The theoretical excitation energies and the experimental UV-vis spectrum of **TCC**. (b) The major electronic transition energies and molecular orbital contributions of **TCC**. Figure S11: The major molecular orbital transitions and excitation energies of **TCC** and the Zn^{2+}-2·**TCC** complex. Figure S12: (a) The theoretical excitation energies and the experimental UV-vis spectrum of the Zn^{2+}-2·**TCC** complex. (b) The major electronic transition energies and molecular orbital contributions of the Zn^{2+}-2·**TCC** complex.

Author Contributions: Conceptualization, B.S. and C.K.; formal analysis, B.S.; investigation, B.S., D.G. and S.Y.; data curation, B.S. and D.G.; writing—original draft preparation, B.S. and D.G.; writing—review and editing, B.S. and C.K.; supervision, C.K. and K.-T.K.; funding acquisition, C.K. and K.-T.K. All authors have read and agreed to the published version of the manuscript.

Funding: The National Research Foundation of Korea (2018R1A2B6001686) is gratefully.

Institutional Review Board Statement: The maintenance of zebrafish was approved by the Institutional Animal Care and Use Committees at the Seoul National University of Science and Technology. Ethical review and approval were waived for this study because early-life stages of zebrafish (<120 hpf) are not protected according to the European Union (EU) Directive 2010/63/EU.

Informed Consent Statement: Not applicable.

Data Availability Statement: Not applicable.

Conflicts of Interest: The authors declare no conflict of interest.

References

1. Yun, D.; Chae, J.B.; So, H.; Lee, H.; Kim, K.T.; Kim, C. Sensing of zinc ions and sulfide using a highly practical and water-soluble fluorescent sensor: Applications in test kits and zebrafish. *New J. Chem.* **2019**, *44*, 442–449. [CrossRef]
2. Qu, W.J.; Guan, J.; Wei, T.B.; Yan, G.T.; Lin, Q.; Zhang, Y.M. A turn-on fluorescent sensor for relay recognition of two ions: From a F^--selective sensor to highly Zn^{2+}-selective sensor by tuning electronic effects. *RSC Adv.* **2016**, *6*, 35804–35808. [CrossRef]
3. Gilbert, R.; Peto, T.; Lengyel, I.; Emri, E. Zinc Nutrition and Inflammation in the Aging Retina. *Mol. Nutr. Food Res.* **2019**, *63*, e1801049. [CrossRef] [PubMed]
4. Kim, M.J.; Kaur, K.; Singh, N.; Jang, D.O. Benzimidazole-based receptor for Zn^{2+} recognition in a biological system: A chemosensor operated by retarding the excited state proton transfer. *Tetrahedron* **2012**, *68*, 5429–5433. [CrossRef]

5. Berg, J.M.; Shi, Y. The galvanization of biology: A growing appreciation for the roles of zinc. *Science* **1996**, *271*, 1081–1085. [CrossRef]
6. Zhang, C.; Liu, Z.; Li, Y.; He, W.; Gao, X.; Guo, Z. In vitro and in vivo imaging application of a 1,8-naphthalimide-derived Zn^{2+} fluorescent sensor with nuclear envelope penetrability. *Chem. Commun.* **2013**, *49*, 11430–11432. [CrossRef]
7. Maity, D.; Govindaraju, T. A differentially selective sensor with fluorescence turn-on response to Zn^{2+} and dual-mode ratiometric response to Al^{3+} in aqueous media. *Chem. Commun.* **2012**, *48*, 1039–1041. [CrossRef]
8. Helal, A.; Rashid, M.H.O.; Choi, C.H.; Kim, H.S. New regioisomeric naphthol-substituted thiazole based ratiometric fluorescence sensor for Zn^{2+} with a remarkable red shift in emission spectra. *Tetrahedron* **2012**, *68*, 647–653. [CrossRef]
9. Vallee, B.L.; Auld, D.S. Zinc Coordination, Function, and Structure of Zinc Enzymes and Other Proteins. *Biochemistry* **1990**, *29*, 5647–5659. [CrossRef]
10. Quang, D.T.; Kim, J.S. Fluoro- and chromogenic chemodosimeters for heavy metal ion detection in solution and biospecimens. *Chem. Rev.* **2010**, *110*, 6280–6301. [CrossRef]
11. Yun, J.Y.; Jo, T.G.; Han, J.; Jang, H.J.; Lim, M.H.; Kim, C. A highly sensitive and selective fluorescent chemosensor for the sequential recognition of Zn^{2+} and S^{2-} in living cells and aqueous media. *Sens. Actuators B Chem.* **2018**, *255*, 3108–3116. [CrossRef]
12. Ploysangam, A.; Falciglia, G.A.; Brehm, B.J. Effect of marginal zinc deficiency on human growth and development. *J. Trop. Pediatr.* **1997**, *43*, 192–198. [CrossRef]
13. Kim, S.; Lee, H.; So, H.; Lee, H.; Kim, K.T.; Kim, C. A benzyl carbazate-based fluorescent chemosensor for detecting Zn^{2+}: Application to zebrafish. *Spectrochim. Acta Part A* **2020**, *228*, 117787–117793. [CrossRef]
14. Chan, W.C.; Saad, H.M.; Sim, K.S.; Lee, V.S.; Ang, C.W.; Yeong, K.Y.; Tan, K.W. A rhodamine based chemosensor for solvent dependent chromogenic sensing of cobalt (II) and copper (II) ions with good selectivity and sensitivity: Synthesis, filter paper test strip, DFT calculations and cytotoxicity. *Spectrochim. Acta Part A* **2021**, *262*, 120099–120112. [CrossRef]
15. Sturgeon, R.E.; Berman, S.S.; Desaulniers, A.; Russell, D.S. Reply to Comments on Determination of Iron, Manganese, and Zinc by Graphite Furnace Atomic Absorption Spectrometry. *Anal. Chem.* **1980**, *52*, 1767–1770. [CrossRef]
16. Antunes, G.A.; Dos Santos, H.S.; Da Silva, Y.P.; Silva, M.M.; Piatnicki, C.M.S.; Samios, D. Determination of Iron, Copper, Zinc, Aluminum, and Chromium in Biodiesel by Flame Atomic Absorption Spectrometry Using a Microemulsion Preparation Method. *Energy Fuels* **2017**, *31*, 2944–2950. [CrossRef]
17. Srivastava, S.K.; Gupta, V.K.; Jain, S. PVC-based 2,2,2-cryptand sensor for zinc ions. *Anal. Chem.* **1996**, *68*, 1272–1275. [CrossRef] [PubMed]
18. Chaiyo, S.; Mehmeti, E.; Žagar, K.; Siangproh, W.; Chailapakul, O.; Kalcher, K. Electrochemical sensors for the simultaneous determination of zinc, cadmium and lead using a Nafion/ionic liquid/graphene composite modified screen-printed carbon electrode. *Anal. Chim. Acta* **2016**, *918*, 26–34. [CrossRef] [PubMed]
19. Ansari, R.; Delavar, A.F.; Mohammad-Khah, A. Solid-state ion selective electrode based on polypyrrole conducting polymer nanofilm as a new potentiometric sensor for Zn^{2+} ion. *J. Solid State Electrochem.* **2012**, *16*, 3315–3322. [CrossRef]
20. Shamsipur, M.; Rouhani, S.; Ganjali, M.R.; Sharghi, H.; Eshghi, H. Zinc-selective membrane potentiometric sensor based on a recently synthesized benzo-substituted macrocyclic diamide. *Sens. Actuators B Chem.* **1999**, *59*, 30–34. [CrossRef]
21. Goswami, S.; Paul, S.; Manna, A. A differentially selective chemosensor for a ratiometric response to Zn^{2+} and Al^{3+} in aqueous media with applications for molecular switches. *RSC Adv.* **2013**, *3*, 25079–25085. [CrossRef]
22. Narayanaswamy, N.; Maity, D.; Govindaraju, T. Reversible fluorescence sensing of Zn^{2+} based on pyridine-constrained bis(triazole-linked hydroxyquinoline) sensor. *Supramol. Chem.* **2011**, *23*, 703–709. [CrossRef]
23. Lee, D.Y.; Singh, N.; Kim, M.J.; Jang, D.O. Ratiometric fluorescent determination of Zn(II): A new class of tripodal receptor using mixed imine and amide linkages. *Tetrahedron* **2010**, *66*, 7965–7969. [CrossRef]
24. Helal, A.; Kim, S.H.; Kim, H. Thiazole sulfonamide based ratiometric fluorescent chemosensor with a large spectral shift for zinc sensing. *Tetrahedron* **2010**, *66*, 9925–9932. [CrossRef]
25. Wei, T.B.; Zhang, P.; Shi, B.B.; Chen, P.; Lin, Q.; Liu, J.; Zhang, Y.M. A highly selective chemosensor for colorimetric detection of Fe^{3+} and fluorescence turn-on response of Zn^{2+}. *Dye. Pigment.* **2013**, *97*, 297–302. [CrossRef]
26. Cheah, P.W.; Heng, M.P.; Saad, H.M.; Sim, K.S.; Tan, K.W. Specific detection of Cu^{2+} by a pH-independent colorimetric rhodamine based chemosensor. *Opt. Mater.* **2021**, *114*, 110990–110997. [CrossRef]
27. Darjee, S.M.; Modi, K.M.; Panchal, U.; Patel, C.; Jain, V.K. Highly selective and sensitive fluorescent sensor: Thiacalix[4]arene-1-naphthalene carboxylate for Zn^{2+} ions. *J. Mol. Struct.* **2017**, *1133*, 1–8. [CrossRef]
28. Bhattacharyya, A.; Ghosh, S.; Makhal, S.C.; Guchhait, N. Hydrazine bridged coumarin-pyrimidine conjugate as a highly selective and sensitive Zn^{2+} sensor: Spectroscopic unraveling of sensing mechanism with practical application. *Spectrochim. Acta Part A* **2017**, *183*, 306–311. [CrossRef]
29. Hwang, S.M.; Kim, C. Fluorescent detection of Zn^{2+} and Cu^{2+} by a phenanthrene-based multifunctional chemosensor that acts as a basic pH indicator. *Inorg. Chim. Acta* **2018**, *482*, 375–383. [CrossRef]
30. Kim, J.H.; Noh, J.Y.; Hwang, I.H.; Kang, J.; Kim, J.; Kim, C. An anthracene-based fluorescent chemosensor for Zn^{2+}. *Tetrahedron Lett.* **2013**, *54*, 2415–2418. [CrossRef]
31. Wechakorn, K.; Suksen, K.; Piyachaturawat, P.; Kongsaeree, P. Rhodamine-based fluorescent and colorimetric sensor for zinc and its application in bioimaging. *Sens. Actuators B Chem.* **2016**, *228*, 270–277. [CrossRef]

32. Gupta, V.K.; Singh, A.K.; Kumawat, L.K. A turn-on fluorescent chemosensor for Zn^{2+} ions based on antipyrine schiff base. *Sens. Actuators B Chem.* **2014**, *204*, 507–514. [CrossRef]
33. Gusev, A.N.; Shul'Gin, V.F.; Meshkova, S.B.; Smola, S.S.; Linert, W. A novel triazole-based fluorescent chemosensor for Zinc ions. *J. Lumin.* **2014**, *155*, 311–316. [CrossRef]
34. So, H.; Cho, H.; Lee, H.; Tran, M.C.; Kim, K.T.; Kim, C. Detection of zinc (II) and hypochlorite by a thiourea-based chemosensor via two emission channels and its application in vivo. *Microchem. J.* **2020**, *155*, 104788–104795. [CrossRef]
35. Vonlanthen, M.; Finney, N.S. Thioureas as reporting elements for metal-responsive fluorescent chemosensors. *J. Org. Chem.* **2013**, *78*, 3980–3988. [CrossRef]
36. Zhu, H.; Fan, J.; Zhang, S.; Cao, J.; Song, K.; Ge, D.; Dong, H.; Wang, J.; Peng, X. Ratiometric fluorescence imaging of lysosomal Zn^{2+} release under oxidative stress in neural stem cells. *Biomater. Sci.* **2014**, *2*, 89–97. [CrossRef]
37. Seo, Y.; Park, S.; Kim, G.; Lee, M.; Kim, C. A naphthyl thiourea-based effective chemosensor for fluorescence detection of Ag^{+} and Zn^{2+}. *Luminescence* **2021**, *36*, 1725–1732. [CrossRef]
38. Chen, Z.E.; Zhang, H.; Iqbal, Z. A new thiosemicarbazone fluorescent probe based on 9,9′-bianthracene for Hg^{2+} and Ag^{+}. *Spectrochim. Acta Part A* **2019**, *215*, 34–40. [CrossRef]
39. Li, Z.; Xiang, Y.; Tong, A. Ratiometric chemosensor for fluorescent determination of Zn^{2+} in aqueous ethanol. *Anal. Chim. Acta* **2008**, *619*, 75–80. [CrossRef]
40. Parr, R.G.; Pearson, R.G. Absolute Hardness: Companion Parameter to Absolute Electronegativity. *J. Am. Chem. Soc.* **1983**, *105*, 7512–7516. [CrossRef]
41. Von Burg, R. Toxicology Update. *J. Appl. Toxicol.* **1992**, *12*, 73–74. [CrossRef]
42. Dzitko, K.; Paneth, A.; Plech, T.; Pawełczyk, J.; Stączek, P.; Stefańska, J.; Paneth, P. 1,4-Disubstituted Thiosemicarbazide Derivatives Are Potent Inhibitors of Toxoplasma Gondii Proliferation. *Molecules* **2014**, *19*, 9926–9943. [CrossRef] [PubMed]
43. Al-Wahaibi, L.H.; Rahul, B.; Mohamed, A.A.B.; Abdelbaky, M.S.M.; Garcia-Granda, S.; El-Emam, A.A.; Percino, M.J.; Thamotharan, S. Supramolecular Self-Assembly Built by Weak Hydrogen, Chalcogen, and Unorthodox Nonbonded Motifs in 4-(4-Chlorophenyl)-3-[(4-fluorobenzyl)sulfanyl]-5-(thiophen-2-yl)-4 H-1,2,4-triazole, a Selective COX-2 Inhibitor: Insights from X-ray and Theoretical Studi. *ACS Omega* **2021**, *6*, 6996–7007. [CrossRef]
44. Kang, J.H.; Han, J.; Lee, H.; Lim, M.H.; Kim, K.T.; Kim, C. A water-soluble fluorescence chemosensor for the sequential detection of Zn^{2+} and pyrophosphate in living cells and zebrafish. *Dye. Pigment.* **2018**, *152*, 131–138. [CrossRef]
45. Frisch, M.J.; Trucks, G.W.; Schlegel, H.B.; Scuseria, G.E.; Robb, M.A.; Cheeseman, J.R.; Scalmani, G.; Barone, V.; Petersson, G.A.; Nakatsuji, H.; et al. *Gaussian 16 Revision C.01*; Gaussian, Inc.: Wallingford, UK, 2016.
46. Becke, A.D. Density-functional thermochemistry. III. The role of exact exchange. *J. Chem. Phys.* **1993**, *98*, 5648–5652. [CrossRef]
47. Lee, C.; Yang, W.; Parr, R.G. Development of the Colle-Salvetti correlation-energy formula into a functional of the electron density. *Phys. Rev. B* **1988**, *37*, 785–789. [CrossRef] [PubMed]
48. Hariharan, P.C.; Pople, J.A. The influence of polarization functions on molecular orbital hydrogenation energies. *Theor. Chim. Acta* **1973**, *28*, 213–222. [CrossRef]
49. Francl, M.M.; Pietro, W.J.; Hehre, W.J.; Binkley, J.S.; Gordon, M.S.; DeFrees, D.J.; Pople, J.A. Self-consistent molecular orbital methods. XXIII. A polarization-type basis set for second-row elements. *J. Chem. Phys.* **1982**, *77*, 3654–3665. [CrossRef]
50. Hay, P.J.; Wadt, W.R. Ab initio effective core potentials for molecular calculations. Potentials for the transition metal atoms Sc to Hg. *J. Chem. Phys.* **1985**, *82*, 270–283. [CrossRef]
51. Wadt, W.R.; Hay, P.J. Ab initio effective core potentials for molecular calculations. Potentials for main group elements Na to Bi. *J. Chem. Phys.* **1985**, *82*, 284–298. [CrossRef]
52. Hay, P.J.; Wadt, W.R. Ab initio effective core potentials for molecular calculations. Potentials for K to Au including the outermost core orbitals. *J. Chem. Phys.* **1985**, *82*, 299–310. [CrossRef]
53. Klamt, A.; Moya, C.; Palomar, J. A Comprehensive Comparison of the IEFPCM and SS(V)PE Continuum Solvation Methods with the COSMO Approach. *J. Chem. Theory Comput.* **2015**, *11*, 4220–4225. [CrossRef] [PubMed]
54. Goswami, S.; Aich, K.; Das, S.; Das Mukhopadhyay, C.; Sarkar, D.; Mondal, T.K. A new visible-light-excitable ICT-CHEF-mediated fluorescence "turn-on" probe for the selective detection of Cd^{2+} in a mixed aqueous system with live-cell imaging. *Dalton Trans.* **2015**, *44*, 5763–5770. [CrossRef] [PubMed]
55. World Health Organization. *WHO Guidelines for Drinking-Water Quality*, 2nd ed.; World Health Organization: Geneva, Switzerland, 1998; Volume 1.
56. Ji, Z.J.; Wu, Y.M.; Wu, F.Y. A ratiometric fluorescence sensor for zinc in neutral solution based on thiourea receptor. *Chem. Lett.* **2006**, *35*, 950–951. [CrossRef]
57. Samanta, S.; Manna, U.; Ray, T.; Das, G. An aggregation-induced emission (AIE) active probe for multiple targets: A fluorescent sensor for Zn^{2+} and Al^{3+} & a colorimetric sensor for $Cu2^{+}$ and F^{-}. *Dalt. Trans.* **2015**, *44*, 18902–18910. [CrossRef]
58. Zhang, C.; Pu, S.; Sun, Z.; Fan, C.; Liu, G. Highly Sensitive and Selective Fluorescent Sensor for Zinc Ion Based on a New Diarylethene with a Thiocarbamide Unit. *J. Phys. Chem. B* **2015**, *119*, 4673–4682. [CrossRef]
59. Gui, Z.; Green, A.R.; Kasrai, M.; Michael Bancroft, G.; Stillman, M.J. Sulfur K-Edge EXAFS Studies of Cadmium-, Zinc-, Copper-, and Silver-Rabbit Liver Metallothioneins. *Inorg. Chem.* **1996**, *35*, 6520–6529. [CrossRef]
60. Deerfield, D.W.; Carter, C.W.; Pedersen, L.G. Models for protein-zinc ion binding sites. II. The catalytic sites. *Int. J. Quantum Chem.* **2001**, *83*, 150–165. [CrossRef]

61. Kshirsagar, N.; Sonawane, R.; Patil, P.; Nandre, J.; Sultan, P.; Sehlangia, S.; Pradeep, C.P.; Wang, Y.; Chen, L.; Sahoo, S.K. Inorganica Chimica Acta Fluorescent chemosensor for Al (III) based on chelation-induced fluorescence enhancement and its application in live cells imaging. *Inorg. Chim. Acta* **2020**, *511*, 119805–119810. [CrossRef]
62. Liu, L.; Shan, D.; Zhou, X.; Shi, H.; Song, B.; Falke, F.; Leinse, A.; Heideman, R. TriPleX^{TM} waveguide-based fluorescence biosensor for multichannel environmental contaminants detection. *Biosens. Bioelectron.* **2018**, *106*, 117–121. [CrossRef]
63. Xing, Y.; Zhu, Q.; Zhou, X.; Qi, P. A dual-functional smartphone-based sensor for colorimetric and chemiluminescent detection: A case study for fluoride concentration mapping. *Sens. Actuators B Chem.* **2020**, *319*, 128254–128261. [CrossRef]